Single microfilaments mediate the early steps of microtubule bundling during preprophase band formation in onion cotyledon epidermal cells

Miyuki Takeuchi[a,b], Ichirou Karahara[c], Naoko Kajimura[d,†], Akio Takaoka[d], Kazuyoshi Murata[e], Kazuyo Misaki[f], Shigenobu Yonemura[f], L. Andrew Staehelin[g], and Yoshinobu Mineyuki[a,*]

[a]Graduate School of Life Science, University of Hyogo, Himeji 671-2201, Japan; [b]Graduate School of Agricultural and Life Sciences, University of Tokyo, Tokyo 113-8657, Japan; [c]Graduate School of Science and Engineering, University of Toyama, Toyama 930-8555, Japan; [d]Research Center for Ultra-High Voltage Electron Microscopy, Osaka University, Ibaraki 567-0047, Japan; [e]National Institute for Physiological Sciences, Okazaki 444-8585, Japan; [f]RIKEN Center for Life Science Technologies, Kobe 650-0047, Japan; [g]Molecular, Cellular and Developmental Biology, University of Colorado, Boulder, CO 80309-0347

ABSTRACT **The preprophase band (PPB) is a cytokinetic apparatus that determines the site of cell division in plants. It originates as a broad band of microtubules (MTs) in G2 and narrows to demarcate the future division site during late prophase. Studies with fluorescent probes have shown that PPBs contain F-actin during early stages of their development but become actin depleted in late prophase. Although this suggests that actins contribute to the early stages of PPB formation, how actins contribute to PPB-MT organization remains unsolved. To address this question, we used electron tomography to investigate the spatial relationship between microfilaments (MFs) and MTs at different stages of PPB assembly in onion cotyledon epidermal cells. We demonstrate that the PPB actins observed by fluorescence microscopy correspond to short, single MFs. A majority of the MFs are bound to MTs, with a subset forming MT-MF-MT bridging structures. During the later stages of PPB assembly, the MF-mediated links between MTs are displaced by MT-MT linkers as the PPB MT arrays mature into tightly packed MT bundles. On the basis of these observations, we propose that the primary function of actins during PPB formation is to mediate the initial bundling of the PPB MTs.**

Monitoring Editor
Manuel Théry
CEA, Hopital Saint Louis

Received: Dec 7, 2015
Revised: Mar 29, 2016
Accepted: Mar 30, 2016

INTRODUCTION

Precise control of the site where the newly formed cell plate attaches to the parental cell walls is essential for plant morphogenesis (Sinnott, 1960). This site is believed to be determined before karyokinesis during preprophase band (PPB) formation (Gunning, 1982). The initial PPB appears during G2 in the form of a broad band of microtubules (MTs), which narrows during the progression of the cell cycle and disappears when the nuclear envelope breaks down (Wick and Duniec, 1983, 1984; Mineyuki *et al.*, 1988). Because the position of the PPB predicts the future division site where the newly formed cell plate is inserted into the parental cell wall at the end of cytokinesis, the PPB is believed to play an essential role in the establishment of the division plane (Mineyuki, 1999). Since their discovery (Pickett-Heaps and Northcote, 1966a,b), PPBs have been observed in many different types of land plants undergoing somatic cell divisions (Mineyuki, 1999). A number of molecules have been localized to PPBs, but how these molecules contribute to PPB MT organization is unclear (McMichael and Bednarek, 2013; Li *et al.*, 2015).

Interactions between the MTs and actins are required for many fundamental processes of animals and plants (Rodriguez et al., 2003; Collings, 2008). Such interactions also appear to play a critical

This article was published online ahead of print in MBoC in Press (http://www.molbiolcell.org/cgi/doi/10.1091/mbc.E15-12-0820) on April 6, 2016.

†Present address: Graduate School of Frontier Biosciences, Osaka University, Osaka 565-0871, Japan.

*Address correspondence to: Yoshinobu Mineyuki (mineyuki@sci.u-hyogo.ac.jp).

Abbreviations used: ADZ, actin-depleted zone; CD, cytochalasin D; MF, microfilament; MT, microtubule; PM, plasma membrane; PPB, preprophase band.

role in PPB formation. The presence of actins in the PPB was first reported in 1987 by three different groups (Kakimoto and Shibaoka, 1987; Palevitz, 1987; Traas *et al.*, 1987). Since then, many other laboratories have confirmed these findings using a variety of fluorescence microscopy techniques, such as immunolabeling, fluorescence-phalloidin labeling, microinjection of fluorescently tagged phalloidin or recombinant actin/actin-interacting molecules in living cells, and visualization of green fluorescent protein–tagged actin-binding-domain proteins in living cells (Lloyd and Traas, 1988; McCurdy *et al.*, 1988; McCurdy and Gunning, 1990; Palevitz, 1988; Katsuta *et al.*, 1990, Katsuta and Shibaoka, 1992; Mineyuki and Palevitz, 1990; Cho and Wick, 1991; Cleary *et al.*, 1992a,b; Cleary, 1995; Cleary and Mathesius, 1996; Eleftheriou and Palevitz, 1992; Liu and Palevitz, 1992; Panteris *et al.*, 1992; Baluska *et al.*, 1997; Zachariadis *et al.*, 2001; Hoshino *et al.*, 2003; Sano *et al.*, 2005; Li *et al.*, 2006; Higaki *et al.*, 2007; Panteris *et al.*, 2007). The presence of F-actin–like microfilaments (MFs) in PPBs has also been observed in electron micrographs (Ding *et al.*, 1991a).

Cells exhibiting an early, broad PPB also possess a broad cortical F-actin array. As the PPB MTs narrows, the actin band narrows, and when the PPB MTs reach their narrowest configuration, the fluorescence signals of actins start to disappear from the cell cortex region occupied by the MT band, giving rise to the actin-depleted zone (ADZ; Cleary *et al.*, 1992b; Liu and Palevitz, 1992). The ADZ forms before the breakdown of the nuclear envelope and persists throughout mitosis (Cleary *et al.*, 1992b; Liu and Palevitz, 1992). At that point, it becomes a negative marker of the future division site.

In addition to the microscopic evidence for cortical actins in the PPB, pharmacological studies have provided indirect evidence for the idea that actin plays a critical role in organizing the PPB MTs. The narrowing of the PPB MTs is prevented by F-actin disrupters such as cytochalasin D (CD; Mineyuki and Palevitz, 1990; Eleftheriou and Palevitz, 1992) and latrunculin A (Granger and Cyr, 2001; Li *et al.*, 2006). These actin disrupters also cause a rebroadening of previously narrowed MT bands (Mineyuki and Palevitz, 1990; Granger and Cyr, 2001; Eleftheriou and Palevitz, 1992). These studies imply that actin is necessary for PPB formation, but how actins interact with MTs during PPB formation remains unknown.

The effect of CD on PPB actin is unique. It is known that cytochalasins block actin polymerization and promote depolymerization of cytoplasmic F-actins. However, the F-actins are not completely depolymerized in CD-treated onion cells (Palevitz, 1988). Indeed, F-actins have been observed in onion root tips and in cotyledon epidermal cells treated with CD (Palevitz, 1988; Mineyuki and Palevitz, 1990). Using improved immunofluorescence techniques, we recently demonstrated that in onion root tip cells treated with 20 μM CD for 30 min, the PPB MT bands of late prophase cells increase in width and actin colocalizes with these broadened PPBs (Takeuchi and Mineyuki, 2014).

To address the question of how F-actins interact with other PPB components requires structural studies with electron microscope–level resolution. MFs bound to interphase cortical MTs have been observed in several ultrastructural studies of chemically fixed plant cells (Seagull and Heath, 1979; Hardham *et al.*, 1980; Heath and Seagull, 1982; Tiwari *et al.*, 1984), as well as in cells preserved by cryofixation/freeze-substitution techniques (Tiwari *et al.*, 1984; Tiwari and Polito, 1988; Lancelle *et al.*, 1987; Ding *et al.*, 1991b; Murata *et al.*, 2002). Single MFs associated with PPBs have been reported in electron micrographs of high-pressure frozen tobacco root tip cells (Ding *et al.*, 1991a). However, the functional significance of this binding has not been explored in a systematic manner. In the present study, we characterize MFs of the PPB by means of electron tomography with high-pressure freezing/freeze substitution techniques. This approach enables us to obtain quantitative information on the number and length of PPB MFs, as well as on the spatial relationship between MFs and MTs in PPBs. We find that ~170-nm-long MFs bind to and cross-link MTs and are involved in MT bundling during early stages of PPB assembly.

RESULTS

We investigated the role of MT-associated MFs in PPB formation in 3-d-old onion cotyledon epidermal cells preserved by high-pressure freezing and freeze-substitution techniques, because PPB assembly and the role of endocytosis in the creation of PPB memory structures in such cells is well characterized (Mineyuki *et al.*, 1989; Mineyuki and Palevitz, 1990; Karahara *et al.*, 2009).

As shown in Figure 1, electron tomography can be used to map the three-dimensional (3D) organization of MT bundles and associated MFs in the cell cortex of PPB-forming cells. Figure 1A is a tomographic slice image of a tangentially sectioned cortical region of an epidermal cell containing a PPB, and Figure 1B shows an electron tomogram–based model of the same PPB. In this model, the thick magenta lines correspond to MTs and the thin yellow lines to MFs. The reconstructed cell cortex region covers an area of ~4 μm^2, and the boxes mark the free MF in Figure 1C and the MT-associated MF in Figure 1D, respectively. Figure 1E shows the planes of the tomographic sections investigated in this study, and Figure 1A corresponds to plane a in Figure 1E.

PPB formation stages can be determined by both nuclear morphology and the width of the PPB in midlongitudinal sections of the cells

To determine the sequential changes in PPB architecture during PPB formation, we staged the cells via nuclear morphology and PPB width in midlongitudinal sections of the cells (Figure 2). Figure 2, A–F, shows the changes in nuclear staining due to differences in chromosome condensation during PPB formation. Typical of interphase nuclei, the nucleus in Figure 2A displays dispersed chromosomes, which give rise to a fine network of darkly staining dots. During prophase, the chromosomes condense into an increasingly coarser dark network, which eventually can be resolved into individual chromosomes during the prophase/prometaphase transition (Figure 2F). In this article, the "late-prophase" cells have nuclei with highly condensed chromatin (Figure 2, D and E) and the "prophase" cells have more-dispersed chromatin (Figure 2, B and C).

The changes in PPB assembly depicted in Figure 2, G–I, illustrate cross-sectional views of the PPB regions in Figure 2, A, E, and F, respectively. The PPB widths were determined using these images. These micrographs demonstrate that the PPB MTs form increasingly larger and tighter bundles as the width of the PPB decreases (compare Figure 2G [PPB width = 10 μm] with Figure 2H [PPB width = 3.6 μm]) and that the number of MTs in a PPB decreases when the cells enter the prophase/prometaphase transition (Figure 2I; PPB width = 3.5 μm). In this study, the process of PPB formation is divided into three stages based on the extent of nuclear condensation and the width of the MT band. Cells with a "prophase" nucleus whose PPB MT width is ≥7 μm are classified as prophase 1 stage cells, cells with a "prophase" nucleus and a narrow PPB (<7 μm) as prophase 2 stage cells, and cells with a nucleus of the "late-prophase" type as late- prophase stage cells. All of the late-prophase cells examined during this study had a narrow PPB.

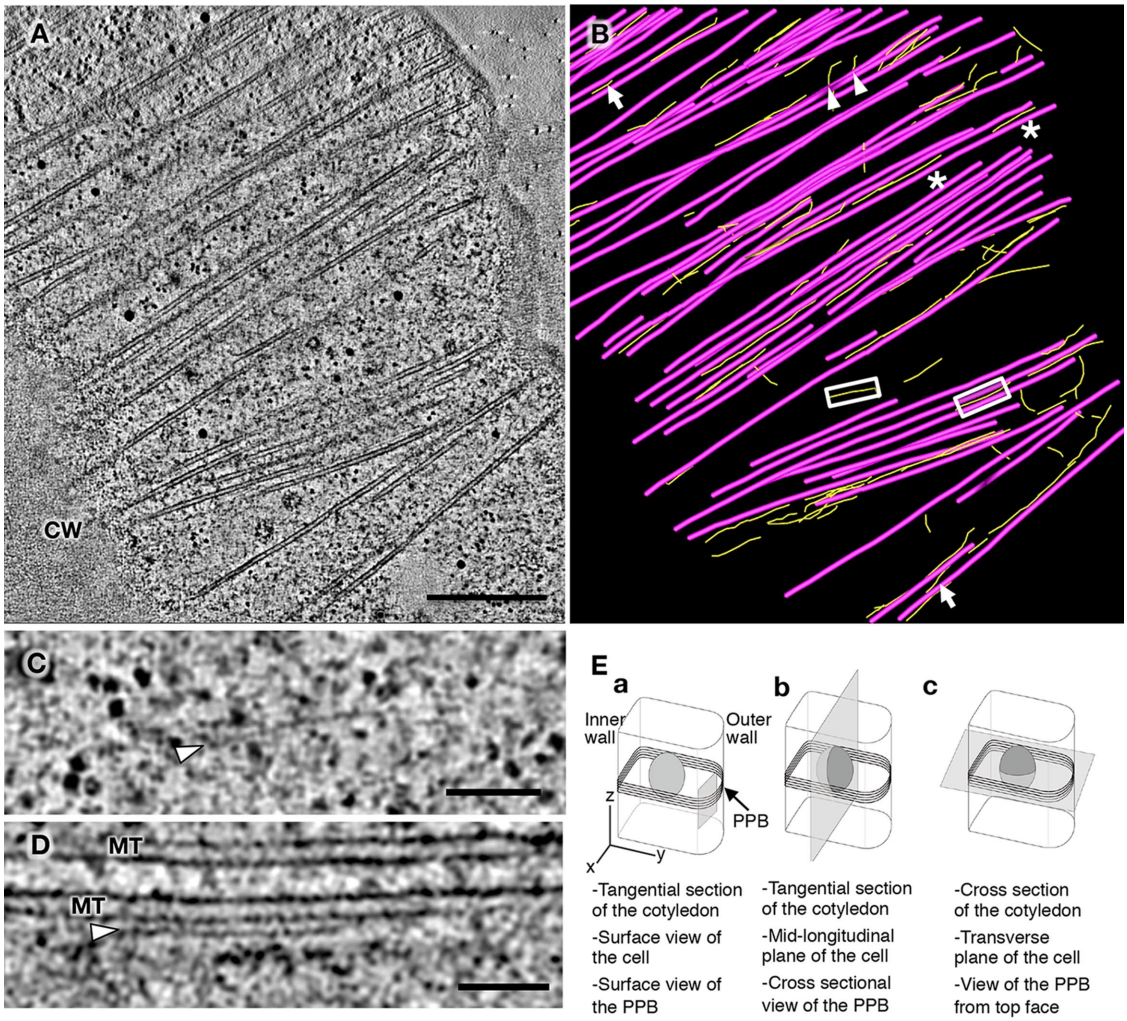

FIGURE 1: Tomographic images and model of MTs and MFs of a tangentially sectioned PPB in an onion cotyledon epidermal cell. (A) Tomographic slice image from tangentially sectioned cell cortex of a prophase cell containing a PPB. CW, cell wall. Bar, 500 nm. (B) Tomography-based reconstruction of the PPB region illustrated in A. The thick magenta lines correspond to MTs and the thin yellow lines to MFs. Arrowheads, contact sites of the end of a MF and that of a MT; arrows, MFs where one end is in contact with a MT and another end is in contact with another MT; asterisks, MFs that run parallel between two MTs and are linked with them by cross-bridging structures (Figure 7, B–F). (C, D) Tomographic slices of images of a single free MF (arrowhead in C) and of a single MF running along a MT (arrowhead in D) highlighted in the boxed areas of B. Bars, 100 nm. (E) Schematic illustrations depicting the plane of the sections used in this study. (a) Tangential section of the cotyledon showing the surface view of the cell. Surface view of the PPB is seen in the *xz*-plane. (b) Tangential section of the cotyledon showing the midlongitudinal plane of the cell. Cross-sectional view of the PPB is seen in the *xz*-plane. (c) Cross-section of the cotyledon showing the transverse plane of the cell. View of the PPB from the top face is seen in the *xy*-plane.

PPB assembly starts with the alignment of cortical MTs and the formation of closely associated MT pairs that coalesce into increasingly large MT clusters

The 3D changes in MT organization and bundling associated with PPB formation are shown in the tomographic models in Figure 3, A–C, which highlight the changes in MT organization during this process. As reported previously (Mineyuki and Palevitz, 1990), most cortical MTs are not organized transversely but instead are distributed randomly in interphase cells of the basal region of the onion cotyledon epidermis (Figure 3A). At the onset of PPB formation, the MTs become organized into loose, irregular arrays oriented at right angles to the longitudinal axis of the cells (Figure 3B). On completion of this MT reorganization stage, groups of two or three MTs initiate the formation of MT bundles by moving closer together and becoming more aligned (Figure 3C). At this stage, the nascent PPBs exhibit their greatest width (~10 µm in the PPB shown in Figure 3C). During the subsequent PPB maturation process, pairs of closely aligned MTs serve as templates for the assembly of increasingly large MT clusters (Figure 1B).

Electron tomography provides the 3D resolution needed to map the spatial relationship between individual MFs and MTs

As shown in Figure 1, electron tomography can provide precise 3D information on the distribution of both MTs and MFs in the PPB

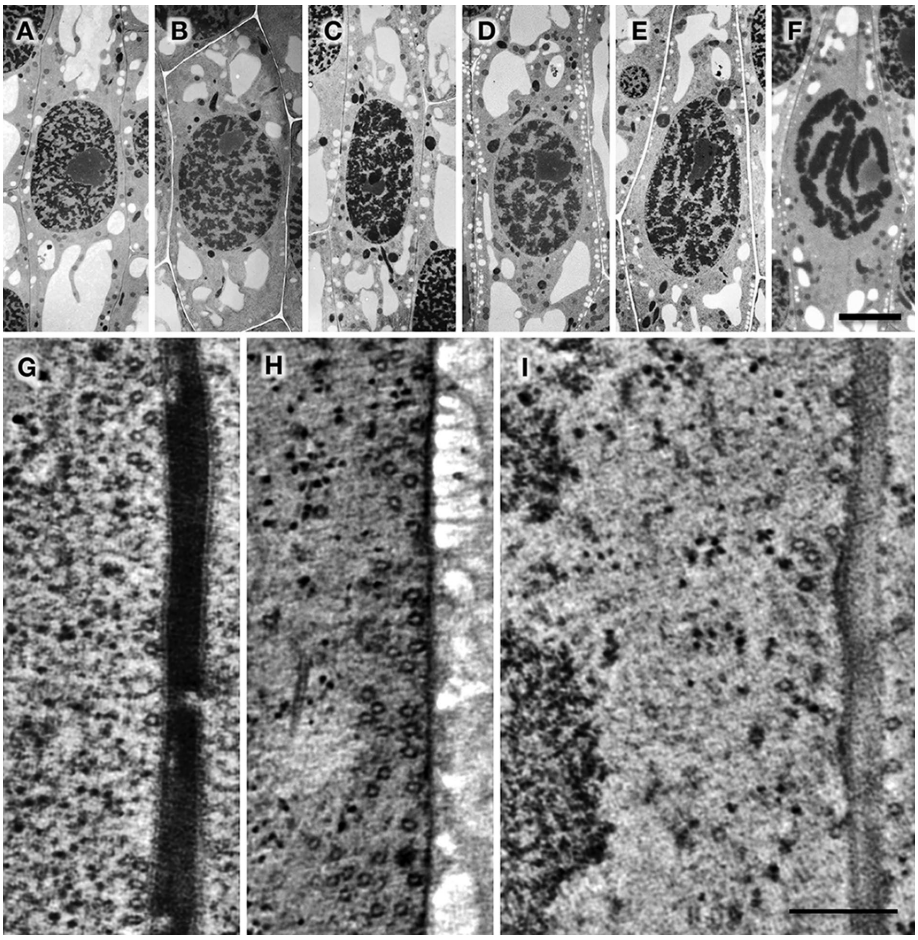

FIGURE 2: Changes in nuclear structure and cortical MT organization in the PPB region of onion cotyledon epidermal cells from interphase to the end of prophase. Electron microscopic images of nuclei (A–F) and PPBs (G–I) in midlongitudinal sections of epidermal cells of onion cotyledons as used for cell cycle staging. (A–F) Nuclei of cells in interphase (A), prophase (B, C), late prophase (D, E), and prophase/prometaphase transition (F). The nuclear staging was based on the extent of chromosome condensation. Bar, 5 μm. (G–I) Cross-sectional views of PPB MTs at different stages of PPB formation. Higher-magnification views of the cortex regions of cells shown in A, E, and F. (G) Initial stage of MT gathering in an early, broad PPB. (H) Late- prophase PPB. (I) Prophase/prometaphase transition stage PPB. PPB width determined for the cells depicted in A–F is 10.0, 9.3, 6.8, 4.5, 3.6, and 3.5 μm, respectively. Bar, 200 nm.

region of onion cotyledon epidermal cells. One of the most striking features of Figure 1B is that whereas the PPB region contains some randomly distributed MFs, most of the MFs appear to be closely associated with MTs, and in many instances, the MFs appear to be laterally connected to a MT. This relationship can be seen in both longitudinal (Figures 1D and 3, E and F) and cross-sectional (Supplemental Figure S1A) views of the MTs. In such images, MTs have a diameter of 25.1 ± 2.6 nm (mean ± SD, $n = 137$), and the associated cross-sectioned MFs, which appear as electron-dense dots have a diameter of 5.9 ± 1.2 nm ($n = 104$), consistent with the expected diameter of F-actins (Supplemental Figure S1E). To demonstrate that the dots marked by arrowheads in Figure S1 A are indeed filaments and not globular protein complexes, we rotated the tomographic images by 90° (Supplemental Figure S1, B–D).

Closer analysis of the MF-MT images shown in Figure 3, E and F, demonstrates that the association of MFs with the MTs is maintained even during MT depolymerization. This is most clearly seen in Figure 3F, where the end of the upper MT displays a horned end (typical of depolymerizing MTs), whereas its associated MF is seen to extend beyond the flaring MT end to the adjacent MT.

Bundled MFs have been observed in electron micrographs of the plant cell cortex in some interphase cells preserved by rapid freezing (e.g., plate 31 in Gunning and Steer, 1996). However, in none of our tomograms of high-pressure frozen cells did we detect any MF bundles in PPBs. All of the PPB MFs we observed were single, relatively short filaments (168 ± 14 nm; mean of the means of nine tomograms ± SE) with a diameter of ~6 nm (Supplemental Figure S1E). This contrasts with the significant number of longer (>500 nm) MFs seen in interphase cell cortex cells, most of which are not bound to MTs (Figure 3A and Supplemental Figure S1F).

In addition to the linear and straight MFs documented in Figures 1, C and D, and 3, D–F, the MTs in the forming PPBs were also associated with short, curved, and branched filamentous structures (Figure 3, H and I, arrowheads). These branched filaments form connections to both cortical MTs and the adjacent plasma membrane (PM; Figure 3, J–M).

The cortical PPB MFs exhibit the same distribution as actin in immunofluorescence studies and are sensitive to CD

If the MFs observed in our tomograms are F-actins, the density of such MFs should decrease significantly in PPB regions of late-prophase cells as the ADZ is formed. Figure 4A illustrates a tomographic model of a late-prophase PPB in which the dense packing of the bundled MTs makes it difficult to discern the associated MFs. Figure 4B omits the MTs and shows only the MFs. As predicted by the ADZ hypothesis, the density of the MFs is reduced within the PPB region (bracketed area) compared with the area outside of the PPB, where the cortical MFs are randomly oriented.

To verify that the MFs in our tomograms are F-actins, we examined the distribution of MFs after subjecting the cells to the F-actin–depolymerizing drug CD. In previous fluorescence microscopy studies (Mineyuki and Palevitz, 1990; Takeuchi and Mineyuki, 2014), we observed that CD did not completely eliminate F-actins from PPBs and that the treatment led to PPB broadening in prophase cells. Our electron tomography data demonstrate the presence of short MFs in the PPBs of CD-treated cells (Figure 4, C and D) and that the CD-induced broadening of the band of PPB MTs (11.6 ± 5.0 μm wide; mean ± SD from three PPBs) is associated with the binding of the shortened MFs to the MTs. In the presence of CD, the average length of the MFs decreased by ~36% compared with control prophase 2–type PPBs (90 vs. 140 nm, mode from histograms). We also observed

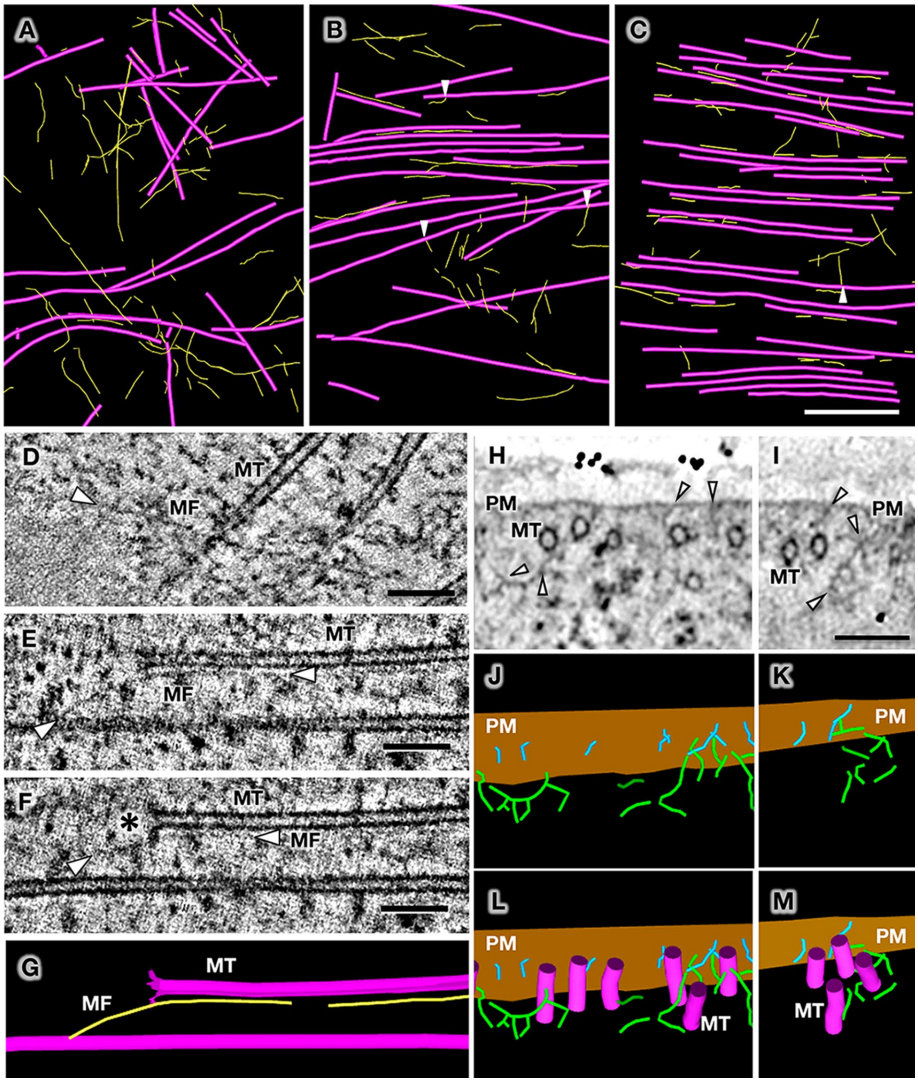

FIGURE 3: Changes in MT-MF association during PPB formation and a gallery of images of cortical MFs and branched MF-like filaments in the PPB region of onion cotyledon epidermal cells. (A–C) Electron tomography models depicting the distribution of MFs and MTs in the cortical cytoplasm of tangentially sectioned cells. Yellow lines and magenta lines show MFs and MTs, respectively. Arrowheads indicate contact sites between a MF end and a MT. Bar, 500 nm. (A) Interphase cell with randomly oriented cortical MTs and MFs. Very few MT-MF interactions are seen. Note the great variability in MF length (there are 92 MFs in this tomogram; length 57–1086 nm, with 14 MFs longer than 500 nm). (B) Interphase cell with some transversely oriented MTs. Note that more MFs are bound to MTs compared with A. (C) Prophase cell with a broad band of PPB MTs (prophase 1). A high proportion of the MFs are bound to MTs. (D–F) Images of MFs (arrowheads) from tomograms of tangentially sectioned cell cortex regions. Bars, 100 nm. (D) A single MF located between the PM and two MTs and which is not aligned with the MTs. (E, F) Two tomographic slice images showing a MF (arrowheads) associated with a depolymerizing MT just beneath the PM. The image in F is ~10 nm below E. In E, the tomographic slice passes close to the top surface of the MT, and the bound MF runs parallel to the MT, whereas the image in F is a midlongitudinal view of the MT, which has a horned end (asterisk). The MF is seen in a grazing view. (G) Tomographic model showing the MF and MTs in E and F. (H, I) MT- and PM-bound, branched and angled MF-like structures in PPBs. The tomograms were reconstructed from tangentially sectioned prophase cells. The arrowheads point to filaments connected to other filaments, MTs, and the PM. Bar, 100 nm. (J, L; K, M) Models of MF-like structures shown in H and I, respectively. The light blue lines correspond to PM-bound, MF-like filaments and the green lines to the other branched and angled MF-like filaments.

that the shortened MFs were unable to form bridges between MTs (Supplemental Figure S2A), and the extent of their binding to MTs appeared to be reduced (Figure 4, C and D).

The length of the MT-associated MFs increases during prophase 1 and reaches a maximum during prophase 2, whereas the MF-to-MT length ratio is greatest in prophase 1 and smallest in late prophase

As evidenced in the tomographic models shown in Figures 1B, 3, and 4, A–D, the spatial organization of MFs and MTs in PPBs undergoes major changes during PPB formation. To further characterize these changes, we determined both the length of the MFs at different stages of PPB formation and the ratio of the length of the MFs to the length of the MTs.

In interphase cells, the MFs are distributed randomly like most of the MTs, and few are associated with MTs (Figure 3A). However, as the MTs assume a transverse orientation and MT bundling starts, a majority of MFs become aligned with, and many become bound to, MTs (Figure 3, B and C). This spatial relationship is maintained through prophase 2 (Figure 1B) until late prophase, when the PPB MFs break down, giving rise to the ADZ (Figure 4). Some of the PPB MFs are connected at only one end to the surface of a MT (arrowheads in Figures 1B and 3, B and C). This type of MF attachment to a MT is also seen in CD-treated PPBs (Figure 4D).

The changes in MF length during these different stages of PPB formation are illustrated in the histograms in Figure 5. During the earliest stages of PPB formation (prophase 1), the MFs are relatively short (mode of histogram 70 nm, average length 126 ± 80 nm; Figure 5A). As the PPB matures, the length of MFs increases to 140 nm (mode) during prophase 2 (Figure 5B) and is maintained at ~140 nm (mode) during late prophase (Figure 5C). The average length of MFs in prophase 2 and late prophase is 187 ± 126 and 178 ± 89 nm, respectively.

Figure 5E highlights a different feature of the relationship between the MT-associated MFs and the MTs, namely the ratio of the total length of the MT-associated MFs to the length of the MTs in PPBs, which provides information on the extent of MF binding to the MTs. The ratio is very low in interphase cells without a PPB. In prophase 1, the ratio is the highest (~0.3), in prophase 2, the ratio drops to ~0.2, and in late prophase, the ratio falls to ~0.07.

MF-mediated bridging of MTs is observed mostly during early stages and the appearance of MT-MT linkers during later stages of PPB development

To elucidate the role of the MT cross-linking structures in PPB formation, we characterized the length, distribution, and timing of the appearance of the different types of MF-MT and MT-MT bridging

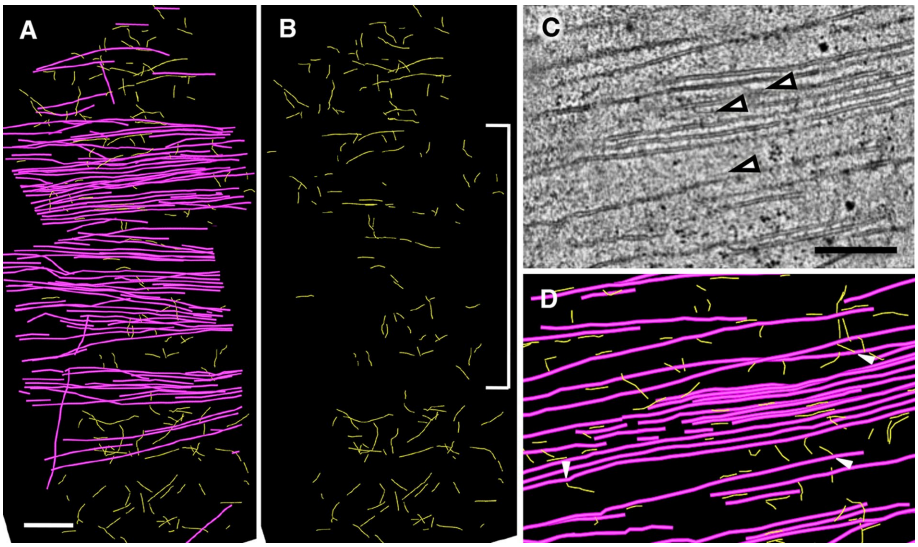

FIGURE 4: Distribution of MFs and MTs in the PPB region of a late-prophase onion cotyledon epidermal cell and effects of CD on PPB structure. Models of MFs and MTs (A) and MFs (B) in which the expected reduction of MFs in the ADZ is clearly visible. (A) Model of a 3.5-μm-wide, late-prophase PPB reconstructed from two tomograms, illustrating the organization of MFs (yellow lines) and MTs (magenta lines). Tomographic images of a tomogram used for this model are shown in Figure 3 of Karahara *et al.* (2009). Bar, 500 nm. (B) Same model as shown in A but without the MT images, to illustrate the difference of MF distribution between the inside and the outside of the PPB. The MF-depleted zone is clearly visible. White bracket indicates the width of the PPB. (C, D) MF fragmentation in a CD-treated late-prophase PPB. (C) Tomographic slice from a tangentially sectioned cell cortex of a CD-treated, late-prophase cell containing broadened-PPB MTs. The onion seedling was incubated with 20 μM CD for 30 min before high-pressure freezing. The PPB width in this cell is 8.7 μm. Bar, 500 nm. (D) MF-MT distribution model reconstructed from the tomogram in C. Thick purple lines show MTs and thin yellow lines MFs. Arrowheads mark the contact sites between the end of MFs and MTs.

structures (Figures 6, A–E, and 7). Based on length measurements from eight tomograms, most MF-MT linkers in prophase 1 were ~14 nm long (13.7 ± 4.4 nm, mean ± SD of 187 MF-MT linkers) and those in late prophase were ~17 nm long (16.7 ± 7.2 nm, mean ± SD of 144 MF-MT linkers). CD had no effect on the length of the MF-MT linkers (Supplemental Figure S3). During early stages of PPB formation, the number of MFs forming bridges between MTs is typically quite low (Figure 3, B and C). However, as the development of the PPBs progresses, the percentage of MFs forming bridges between MTs increases significantly (Figure 1). MFs running between two adjacent MTs can form connections to both MTs, but the linkers to the two MTs are not in the same plane (Figure 6, B–F).

In contrast to the MT-MF linkers, the length of the MT-MT linkers is more variable (Figure 7, A–E). The mean length of all of the MT-MT linkers was 25.3 ± 9.9 nm (mean ± SD from 1109 linkers from 10 tomograms), but the shortest linkers were only ~30% (Figure 7C) of the length of the longest ones (Figure 7D). Because we were not able to discern individual peaks in the MT-MT linker length histogram of all linkers, we determined the length distribution for each stage of PPB development (Figure 7, F–H). Although few in number, distinct, >50-nm bridge structures (Figure 7D) were seen in all PPB developmental stages. The histogram of prophase 1 cells (Figure 7F) exhibits a typical Gaussian distribution with a peak of ~27 nm and average length of 29.0 ± 9.3 nm. This is the stage during which groups of two to three MTs begin to form bundles (Figure 8A). As the small MT bundles start to coalesce into MT clusters during prophase 2 (Figure 8B), the average length of the linkers decreases to ~25 nm (Figure 7G). The linker-length histogram of late prophase cells (Figure 7H) exhibits a typical Gaussian distribution with a peak of ~23 nm. During this phase, the small MT clusters consolidate into large MT clusters. At the end of late prophase, a PPB typically consists of two or three large, 3D MT clusters with each composed of ~30 MTs held together by MT-MT linkers. These bundled PPB MTs are also tethered to the PM via cross-bridges between PM and MTs (Figure 6, G–I, and Supplemental Figure S4).

DISCUSSION

Our electron tomography study of high-pressure frozen/freeze-substituted PPBs in onion cotyledon epidermal cells shows that PPBs contain two types of filamentous structures—single, linear, 6-nm filaments (MFs), which are often bound to MTs and run parallel to the plane of the PM (Figures 1, C and D, 3, D–F, and 6, A–D, and Supplemental Figure S1, A–D and F), and short, branched, and angled MF-like structures that form links between the MTs and the PM (Figure 3, H and I). The single, linear MFs appear to correspond to F-actins that have been predicted to exist based on various types of fluorescence microscopy studies (see *Introduction*), whereas the identity of the branched structures is unknown.

The single MFs start to associate with MTs during the onset of PPB assembly (Figure 3, A–C), and both the number and length of the MT-associated MFs increase during prophase 2 (Figures 1 and 5). A significant drop in the number of MFs was observed in late prophase PPBs (Figure 4, A and B). These changes in MF distribution and number during PPB formation correlate with the appearance of PPB actins during early stages of PPB development and the loss of actin documented by immunofluorescence microscopy during late prophase (Liu and Palevitz, 1992; Takeuchi and Mineyuki, 2014). The CD-induced redistribution of MFs in late-prophase PPBs (Figure 4, C and D) matches the changes in F-actin distribution in the CD-treated and rebroadened PPBs shown by fluorescence microscopy (Mineyuki and Palevitz, 1990; Takeuchi and Mineyuki, 2014). Together, these results support the idea that the PPB-associated single MFs are F-actins, although we cannot formally claim that the MFs in the tomograms are F-actins.

In the present study, we characterize the single MFs in terms of their 3D organization and spatial relationship to the PPB MTs. We also present quantitative information on their length. Our measurements show that most MT-associated MFs are relatively short, ~70 nm (mode) in prophase 1 and ~140 nm (mode) in prophase 2 and late prophase (Figure 5). These results suggest that the initial step of PPB formation involves the binding of short MF fragments to the MTs (arrowheads in Figures 1B, 3, B and C, 4D, and 9A), followed by MF elongation along the MTs, possibly mediated or enhanced by the linkers, during prophase (Figure 9B). Live-cell imaging demonstrated that F-actins start to elongate along cortical MTs after washout of latrunculin B in interphase cells (Sampathkumar *et al.*, 2011). This type of growth may also occur during early stages of PPB formation (Figure 9, A–C).

In contrast to the short MFs in the PPB, longer MFs were also frequently observed in the interphase cells of our samples (Figure 3A

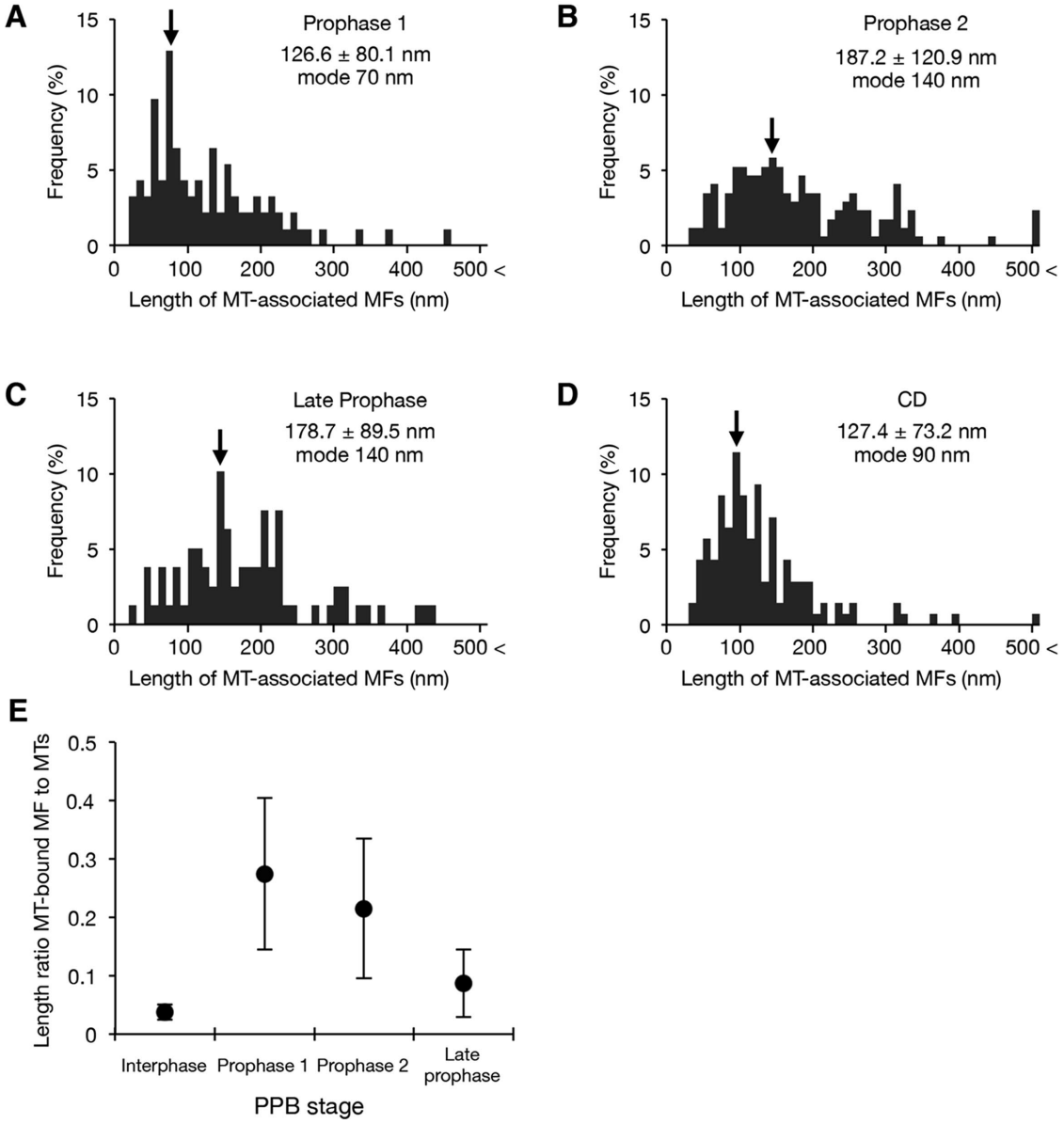

FIGURE 5: Changes in the length and frequency of MT-associated MFs during PPB formation and in response to CD treatment in onion cotyledon epidermal cells. (A–C) Histograms showing the distribution of MF length in PPBs of prophase 1 (A), prophase 2 (B), and late-prophase (C) stages. (D) MF length distribution in the broadened PPBs of CD-treated cells. Onion seedlings were incubated with 20 μM CD for 30 min before high-pressure freezing. Cells used for the tomograms were late prophase and possessed broad MT bands. Mean ± SD of the length of MFs and the mode of the length of MFs are shown in each column. The mode of each histogram is marked by an arrow. The numbers of MFs used for the histograms in A–D were 93, 172, 79, and 140, respectively. (E) Changes in the ratio of the total length of the MT-associated MFs to that of the MTs in PPBs during PPB formation. Cells were divided into four groups according to nuclear stages and PPB width: interphase (interphase cell without a PPB), prophase1 (prophase cell with a broad PPB whose width is ≥7 μm), prophase 2 (prophase cell with a narrow PPB whose width is <7 μm), and late prophase (a late-prophase cell with a PPB). The extent of MFs associated with MTs was determined by measuring the total length of the MT-associated MFs to the total length of the MTs in each stage. Mean ± SD is shown in each group. Data points were calculated from three interphase, six prophase 1, four prophase 2, and six late-prophase tomograms.

and Supplemental Figure S1F), as reported in pollen tubes (Lancelle *et al.*, 1987) and tobacco interphase cells (Ding *et al.*, 1991b). This implies that the MFs in the PPB are maintained in a short configuration for their function. Possible candidate proteins for keeping MFs short include a heterodimeric MF capping protein that binds tightly to the barbed ends of F-actins in *Arabidopsis* (Huang *et al.*, 2003, 2006; Li *et al.*, 2012) and F-actin–severing proteins such as ADF/cofilin (Staiger and Cande, 1991; Staiger *et al.*, 2010).

Analysis of the changes in MT clustering during PPB formation (Figure 8) shows that the MT band-narrowing process can be divided into three stages: 1) formation of MT pairs to initiate MT bundle formation, 2) organization of the MT bundles into loose MT clusters,

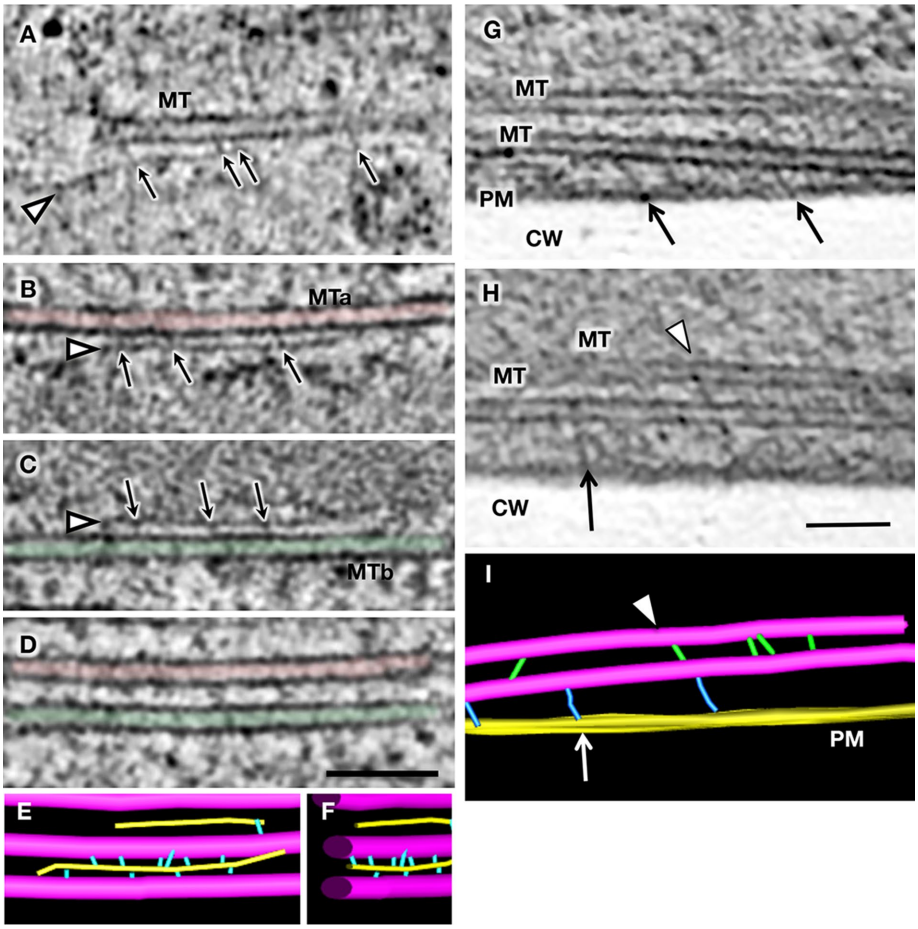

FIGURE 6: Gallery of images of MF-MT and MT-PM bridges during PPB formation of onion cotyledon epidermal cells. (A) Tomographic slice view of a PPB showing a MF (arrowhead) associated with a MT. The MF is connected to the MT by cross-bridging structures (arrows). (B–D) Three tomographic slices from a small volume of a PPB. The volume contains two MTs and a MF. Images A–F are at the same magnification. Bars, 100 nm. (B, C) The single MF (arrowhead) is bound to two adjacent MTs—MTa (B) and MTb (C)—via cross-bridges (arrows). The image in C is a tomographic slice tilted ~60° around the axis of the MF depicted in B. (D) Another view of the volume illustrated in B and C. The MF cannot be seen in this plane; instead, the image was chosen to highlight the parallel arrangement of MTa and MTb. (E, F) Tomographic models of the arrangement of the two MTs (green and red) and one MF illustrated in B–D. Magenta, MTs; yellow, MF; light blue, MT-MF bridges. The two MTs are bundled via linkers to the single MF. Note that the centers of the two MTs and MF are not on the same plane. (G–I) Anchoring of bundled MTs to PM in a late-prophase PPB. (G, H) Tomographic slices of a 500-nm-thick mid cross-section showing MTs running along PM. CW, cell wall. The MT- PM (arrows) and MT-MT (arrowhead) linkers have different lengths. Bar = 100 nm. (I) A tomographic model showing the MF, MTs, PM, and cross-bridges in H. The length of the bridging structures between PM and MTs varied from 20 to 60 nm.

and 3) reduction of the MT-MT spacing to form tight MT clusters. As demonstrated in Figures 3, 4, and 6, the early events of PPB assembly appear to be mediated by MF bridging structures, whereas the latter ones involve different types of MT-MT linkers (Figure 7). On the basis of these data, we developed the PPB assembly model shown in Figure 9.

The actin-mediated events of PPB assembly start with the binding of short (~70 nm) MFs to the MTs and the subsequent alignment of the MFs with the MTs as more linkers connect the two structures (Figures 1B, 3, B and C, and 9, A and B). Whether these events involve one or two types of MF-MT linkers has yet to be determined. During prophase 2, lengthening of the bound MFs (Figure 5, A and B) enables them to form bridges between MTs that are separated by spaces that are too big to be bridged by MT-MT linker proteins (Figures 1B, 3, E–G, and 9, C and D). As the zippering up of the MF-linked MTs continues, the MTs come closer together, with the MFs becoming sandwiched between the two parallel MTs to which they are connected via alternating cross-links (Figures 6, B–F, and 9E). As this occurs, the MF-mediated cross-links are replaced by direct MT-MT bridging structures (Figures 7 and 9, F and G, and Supplemental Figure S4).

Our observations show that single MFs bound to MTs play an essential role in MT bundling during early stages of PPB formation. The linkers that connect the MFs to the PPB MTs are ~15 nm long. Cross-bridges 10–15 nm long have been observed connecting single MFs and MTs in tobacco pollen tubes and tissues preserved by cryofixation/freeze-substitution techniques (Lancelle *et al.*, 1987; Ding *et al.*, 1991b). The demonstration that F-actin fragments are translocated along MTs (Sampathkumar *et al.*, 2011) in jasplakinolide-treated interphase cells suggests an interesting mechanism for bringing F-actins attached to one MT into contact with a second MT, so that the MTs can become cross-linked by an F-actin bridge. Molecules capable of forming cross-links between F-actins, and MTs have an actin-binding domain at one end and a MT-binding motif at the other, or they can be composed of a protein complex with one subunit having an actin-binding motif and the second having a MT-binding motif (Petrasek and Schwarzerova, 2009). Candidate motor proteins for this activity include the kinesin-14 protein family with actin-binding, calponin-homology domains (KCHs; reviewed in Schneider and Persson, 2015). Members of the KCH protein family capable of forming MF-MT cross-bridges have been identified in a variety of plant species and tissues: cotton fibers (GhKCH1, Preuss *et al.*, 2004; GhKCH2, Xu *et al.*, 2009), rice coleoptiles (OsKCH1; Frey *et al.*, 2009), and tobacco cells (Frey *et al.*, 2009). In addition, two kinesin-14 family proteins (NtKCH [Klotz and Nick, 2012] and KingG [Buschmann *et al.*, 2011]) localize to PPBs. The formin isoform AFH14 of *Arabidopsis* has been detected in PPBs and suggested to interact with both actin and MTs, as shown by in vitro experiments and knockdown of AFH14 in mitotic cells (Li *et al.*, 2010).

Based on their length, PPB MT-MT linkers can be divided into two groups: MAP-M, the dominant type in prophase 1, and MAP-S, the major one in late prophase (Figures 7 and 9). MAP-M is replaced by MAP-S linkers during MT band narrowing. Several MT-associated proteins have been localized to PPBs (McMichael and Bednarek, 2013; Hamada, 2014). Further studies are necessary to

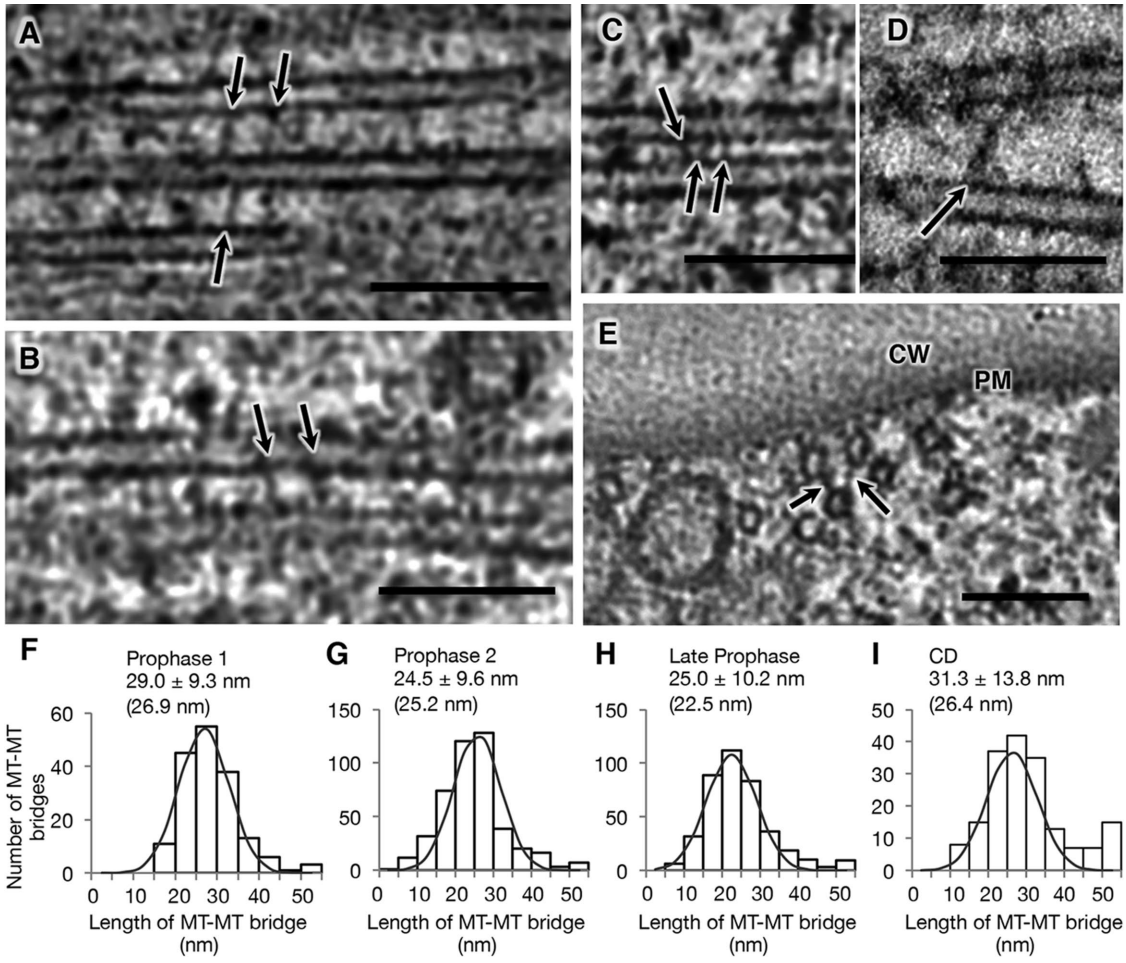

FIGURE 7: Gallery of images of MT-MT bridges and length–distribution histograms of MT-MT bridges during PPB formation of onion cotyledon epidermal cells. (A–E) MT-MT bridges in PPBs. Bars, 100 nm. (A–D) Tomographic slices from tangential sections through PPBs. The arrows point to bridging structures between adjacent MTs. The lengths of the bridges in A–D are 30, 20, 12, and 57 nm, respectively. (E) A tomographic slice from tangential sections showing a cross-sectional view of a PPB. A cluster of MTs is seen beneath the PM, and bridging structures between the MTs are evident (arrows). CW, cell wall. (F–I) Comparison of the length of MT-MT bridges in PPBs of prophase 1 (F), prophase 2 (G), and late prophase (H) and that in CD-treated late-prophase PPBs (I) from two, four, three, and four tomograms, respectively. The mean ± SD is shown in each column. Each developmental stage is explained in Figure 5. For CD treatment, onion seedlings were incubated with 20 μM CD for 30 min before high-pressure freezing, and the cells used for tomograms were late prophase and all possessed wide MT bands. Analysis of the length distribution was performed by using PeakFit software with a Gaussian distribution function with $R^2 = 0.99$ in the case of cells in early prophase 1 or prophase and 0.91 and 0.96 in early prophase 2 and CD, respectively. The number in parentheses in each column shows the value of the peak. The fitted curves suggest that the dominant size of the bridges was 26.9 nm in prophase 1 and 22.5 nm in late prophase. A significant difference was found between the distributions of F and H (Kolmogorov–Smirnov test, two-tailed, $p < 0.01$).

identify the MAPs that correspond to the MAP-M and MAP-S structures.

MATERIALS AND METHODS

Plant material

Onion (*Allium cepa* L. cv. Highgold Nigou; Sakata Seed, Yokohama, Japan) seeds were sown on pieces of filter paper soaked with 0.05 M sucrose in water. They were grown in the dark at 25°C for 2 d. Seedlings were transferred to 0.1 M sucrose in water and cultured for 1 d. For CD treatment, the 3-d-old seedlings were incubated on 20 μM CD solution containing 0.1% (vol/vol) dimethyl sulfoxide (DMSO) for 30 min in the dark. CD was obtained from Sigma-Aldrich (St. Louis, MO), and 20 mM stock dissolved in DMSO was kept at –20°C until use.

Sample preparation for high-pressure freezing and freeze substitution

Three-day-old seedlings were used for sample preparation by high-pressure freezing and freeze substitution following the method described in Murata *et al*. (2002). Briefly, 3-mm-long basal parts of the cotyledons were cut from the onion seedlings and immediately frozen using a high-pressure freezer (BAL-TEC HPM 010; Bal-Tec, Balzers, Liechtenstein; now Leica, Wetzlar, Germany). The 0.1 M sucrose dissolved in water was used as cryoprotectant.

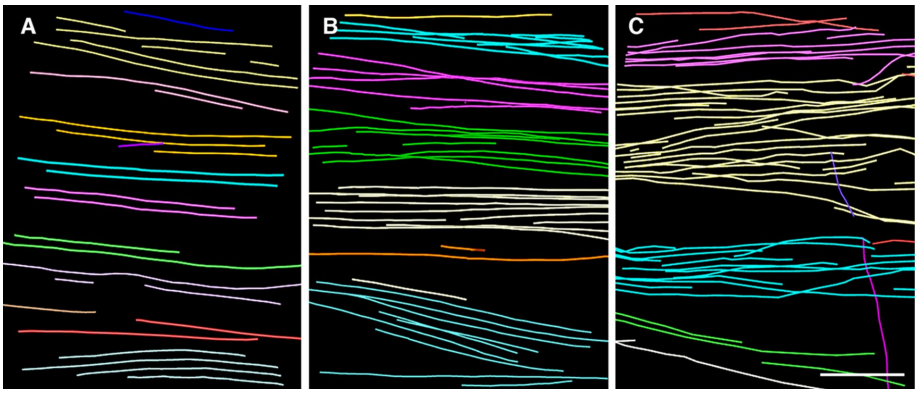

FIGURE 8: Changes in MT-bundle cluster sizes during PPB formation in onion cotyledon epidermal cells. (MT-distribution models from tomograms of PPBs in tangentially sectioned cell cortex in prophase 1 (A), prophase 2 (B), and late prophase (C). The colored lines correspond to individual MTs. MTs that were connected each other via MT-MT bridges are shown in the same MT color. Bar, 500 nm.

The high-pressure frozen tissues were freeze-substituted in 2% OsO_4 in acetone at –80°C for 3 d, at –20°C for 1 d, at 4°C overnight, and at room temperature for 2 h. After the incubation of samples with 2% (wt/vol) OsO_4 solution at 40°C for 2 h, the samples were treated with 5% uranyl acetate in methanol at 4°C for 2 h. After being washed with methanol and acetone at room temperature, they were infiltrated with a graded series of Spurr's resin (Polysciences, Warrington, PA). Polymerization was performed at 70°C for 16 h.

Specimen preparation for electron tomography

We prepared serial tangential sections and serial cross-sections of epidermal cells from the embedded tissues for quantitative analysis. Tangential sections of PPBs (Figure 1Ea) were used to analyze MF-MT relationships, and cross-sectional views (Figure 1Eb) were used to determine nuclear stages and PPB width. Cross-sections were also used to analyze MT-MT and MT-PM linkers. Serial tangential sections (250 nm thick) of epidermal cells were prepared from the embedded tissues. The sections were mounted on Formvar-coated slot grids. Each series of sections contained 50–100 serial sections and included midlongitudinal plane and outer surface wall sections of the cells. Sections containing longitudinal plane views of the nuclei were examined in a transmission electron microscope (JEOL 1010; JEOL, Akishima, Japan) to identify prophase cells. Prophase cells were distinguished by the condensation level of chromosomes (Figure 2). Once a prophase cell was identified, the other sections were examined to find a section with a midlongitudinal view of the nucleus and the corresponding cross-sectional view of the PPB, as well as a tangential section through the cell cortex for a tangential view of the PPB. PPB width was determined on the section containing the midlongitudinal view of the nucleus. Serial cross-sections (500 nm thick) were cut at the level of the nuclei, and sections containing MTs in an outer cortical region of the target prophase cell were processed for electron tomography.

Electron tomography

The sections were double stained with 2% (wt/vol) uranyl acetate in 60% (vol/vol) methanol and Reynold's lead citrate, and then colloidal gold particles were added to both sides of the grids. The gold particles were used as fiducial markers to align series of tilted images. We used 10-nm colloidal gold particles (BBI Solutions, Cardiff, United Kingdom) for 250-nm-thick sections and 25-nm colloidal gold particles conjugated with bovine serum albumin (AURION, Wageningen, Netherlands) for 500-nm-thick sections. For dual-axis electron tomography, the 250-nm-thick tangential sections were observed using a Hitachi H-9500 (Hitachi, Tokyo, Japan) operating at 300 kV, a TF30 intermediate-voltage Tecnai EM (FEI, Tokyo, Japan) operating at 300 kV, or a JEM-1000 high-voltage microscope (JEOL) operating at 750 kV. The images were taken from 60° to –60° tilt with 1° increments about two orthogonal axes. When a Hitachi H-9500 was used, the images were taken at 15,000× with a resolution of 2048 × 2048 pixels at a pixel size of 1.23 nm using an F224HD charge-coupled device camera (TVIPS, Gauting, Germany). The detailed operating conditions for TF30 and JEM-1000 are described elsewhere (Karahara *et al.* 2009). For single-axis tomography of 500-nm-thick sections, images were obtained using an H-1250M (Hitachi) operating at 1000 kV, and the images were taken at 10,000×. The images on films were scanned at 4000 dpi and used for image processing. Tomograms were generated from the tilted image series, and the tomograms were analyzed with IMOD, which is a group of programs for 3D reconstruction and modeling (Kremer *et al.* 1996). Twenty tomograms of intact cells and four tomograms of CD-treated cells were used.

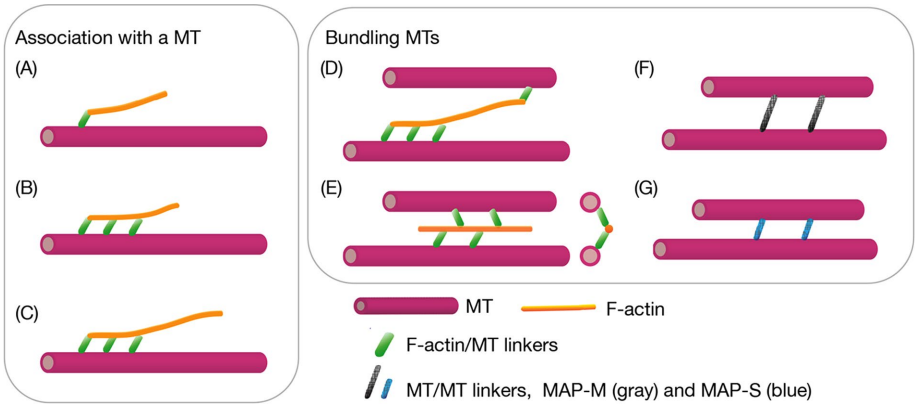

FIGURE 9: Model showing how single F-actins contribute to MT bundling during the early stages of PPB and are replaced during later stages by MT-MT linkers. (A) PPB formation starts when one end of a short F-actin fragment attaches to a MT via a linker protein. (B) The F-actin fragment aligns along the MT by linkers. (C) The short F-actin fragment bound to the MT elongates. (D) The free end of the MT-associated F-actin extends to a neighboring MT, to which it becomes attached. (E) Addition of more MF-MT cross-links pulls the MTs together until they form zipper-like structures where the MF is connected to the two MTs through alternating linkers. This tight coupling enables the two MTs to become cross-linked through short MT-MT bridges. (F, G) The MT-MT bridges are formed by MAPs with different lengths. In earlier stages, the longer MAPs are more numerous, whereas in prophase 2 and late prophase, the shorter MAPs become the dominant form.

ACKNOWLEDGMENTS

Part of this work was supported by the Advanced Characterization Nanotechnology Platform, Nanotechnology Platform Program of the Ministry of Education, Culture, Sports, Science and Technology (MEXT), Japan, at the Research Center for Ultra-High Voltage Electron Microscopy (Nanotechnology Open Facilities) at Osaka University and by the Cooperative Study Program of the National Institute for Physiological Sciences. This work was also partly supported by Japan Society for the Promotion of Science Grant 17207006 and MEXT Grant 17049019 to Y.M.

REFERENCES

Baluska F, Vitha S, Barlow PW, Volkmann D (1997). Rearrangements of F-actin arrays in growing cells of intact maize root apex tissues: a major developmental switch occurs in the postmitotic transition region. Eur J Cell Biol 72, 113–121.

Buschmann H, Green P, Sambade A, Doonan JH, Lloyd CW (2011). Cytoskeletal dynamics in interphase, mitosis and cytokinesis analysed through agrobacterium-mediated transient transformation of tobacco BY-2 cells. New Phytol 190, 258–267.

Cho SO, Wick SM (1991). Actin in the developing stomatal complex of winter rye: a comparison of actin antibodies and Rh-phalloidin labeling of control and CB-treated tissues. Cell Motil Cytoskeleton 19, 25–36.

Cleary AL (1995). F-actin redistributions at the division site in living tradescantia stomatal complexes as revealed by microinjection of rhodamine-phalloidin. Protoplasma 185, 152–165.

Cleary AL, Brown RC, Lemmon BE (1992a). Microtubule arrays during mitosis in monoplastidic root tip cells of *Isoetes*. Protoplasma 167, 123–133.

Cleary AL, Gunning BES, Wasteneys GO, Hepler PK (1992b). Microtubule and F-actin dynamics at the division site in living *Tradescantia* stamen hair-cells. J Cell Sci 103, 977–988.

Cleary AL, Mathesius U (1996). Rearrangements of F-actin during stomatogenesis visualised by confocal microscopy in fixed and permeabilised *Tradescantia* leaf epidermis. Bot Acta 109, 15–24.

Collings DA (2008). Crossed-wires: interactions and cross-talk between the microtubule and microfilament networks in plants. In: Plant Microtubules, ed. P Nick, Vol. 11, Berlin: Springer, 47–79.

Ding B, Turgeon R, Partharathy MV (1991a). Microfilament organization and distribution in freeze substituted tobacco plant tissues. Protoplasma 165, 96–105.

Ding B, Turgeon R, Partharathy MV (1991b). Microfilaments in the preprophase band of freeze substituted tobacco root cells. Protoplasma 165, 209–211.

Eleftheriou EP, Palevitz BA (1992). The effect of cytochalasin D on preprophase band organization in root tip cells of *Allium*. J Cell Sci 103, 989–998.

Frey N, Klotz J, Nick P (2009). Dynamic bridges—a calponin-domain kinesin from rice links actin filaments and microtubules in both cycling and non-cycling cells. Plant Cell Physiol 50, 1493–1506.

Granger C, Cyr R (2001). Use of abnormal preprophase bands to decipher division plane determination. J Cell Sci 114, 599–607.

Gunning BES (1982). The cytokinetic apparatus: Its development and spatial regulation. In: The Cytoskeleton in Plant Growth and Development, ed. CW Lloyd, London: Academic Press, 229–292.

Gunning BES, Steer MW (1996). Plant Cell Biology: Structure and Function, Burlington, MA: Jones & Bartlett Learning.

Hamada T (2014). Microtubule organization and microtubule-associated proteins in plant cells. Int Rev Cell Mol Biol 312, 1–52.

Hardham AR, Green PB, Lang JM (1980). Reorganization of cortical microtubules and cellulose deposition during leaf formation in *Grapetopetalum paraguayense*. Planta 149, 181–195.

Hardham AR, Gunning BE (1978). Structure of cortical microtubule arrays in plant cells. J Cell Biol 77, 14–34.

Heath IB, Seagull RW (1982). Oriented cellulose fibrils and the cytoskeleton: a critical comparison of models. In: The Cytoskeleton and Plant Growth and Development, ed. CW Lloyd, London: Academic Press, 163–182.

Higaki T, Sano T, Hasezawa S (2007). Actin microfilament dynamics and actin side-binding proteins in plants. Curr Opin Plant Biol 10, 549–556.

Hoshino H, Yoneda A, Kumagai F, Hasezawa S (2003). Roles of actin-depleted zone and preprophase band in determining the division site of higher-plant cells, a tobacco BY-2 cell line expressing GFP-tubulin. Protoplasma 222, 157–165.

Huang S, Blanchoin L, Kovar DR, Staiger CJ (2003). *Arabidopsis* capping protein (AtCP) is a heterodimer that regulates assembly at the barbed ends of actin filaments. J Biol Chem 278, 44832–44842.

Huang S, Gao L, Blanchoin L, Staiger CJ (2006). Heterodimeric capping protein from *Arabidopsis* is regulated by phosphatidic acid. Mol Biol Cell 17, 1946–1958.

Kakimoto T, Shibaoka H (1987). Actin filaments and microtubules in the preprophase band and phragmoplast of tobacco cells. Protoplasma 140, 151–156.

Karahara I, Suda J, Tahara H, Yokota E, Shimmen T, Misaki K, Yonemura S, Staehelin LA, Mineyuki Y (2009). The preprophase band is a localized center of clathrin-mediated endocytosis in late prophase cells of the onion cotyledon epidermis. Plant J 57, 819–831.

Katsuta J, Hashiguchi Y, Shibaoka H (1990). The role of the cytoskeleton in positioning of the nucleus in premitotic tobacco BY-2 cells. J Cell Sci 95, 413–422.

Katsuta J, Shibaoka H (1992). Inhibition by kinase inhibitors of the development and the disappearance of the preprophase band of microtubules in tobacco BY-2 cells. J Cell Sci 103, 397–405.

Klotz J, Nick P (2012). A novel actin-microtubule cross-linking kinesin, NtKCH, functions in cell expansion and division. New Phytol 193, 576–589.

Kremer JR, Mastronarde DN, McIntosh JR (1996). Computer visualization of three-dimensional image data using IMOD. J Struct Biol 116, 71–76.

Lancelle SA, Cresti M, Hepler PK (1987). Ultrastructure of the cytoskeleton in freeze-substituted pollen tubes of *Nicotiana alata*. Protoplasma 140, 141–150.

Li CL, Chen ZL, Yuan M (2006). Actomyosin is involved in the organization of the microtubule preprophase band in *Arabidopsis* suspension cultured cells. J Integr Plant Biol 48, 53–61.

Li J, Pleskot R, Henty-Ridilla JL, Blanchoin L, Potocky M, Staiger CJ (2012). Arabidopsis capping protein senses cellular phosphatidic acid levels and transduces these into changes in actin cytoskeleton dynamics. Plant Signal Behav 7, 1727–1730.

Li S, Sun T, Ren H (2015). The functions of the cytoskeleton and associated proteins during mitosis and cytokinesis in plant cells. Front Plant Sci 6, 282.

Li Y, Shen Y, Cai C, Zhong C, Zhu L, Yuan M, Ren H (2010). The type II *Arabidopsis* formin14 interacts with microtubules and microfilaments to regulate cell division. Plant Cell 22, 2710–2726.

Liu B, Palevitz BA (1992). Organization of cortical microfilaments in dividing root cells. Cell Motil Cytoskeleton 23, 252–264.

Lloyd CW, Traas JA (1988). The role of F-actin in determining the division plane of carrot suspension cells. Drug studies. Development 102, 211–221.

McCurdy DW, Gunning BES (1990). Reorganization of cortical actin microfilaments and microtubules at preprophase and mitosis in wheat root-tip cells—a double label immunofluorescence study. Cell Motil Cytoskeleton 15, 76–87.

McCurdy DW, Sammut M, Gunning BES (1988). Immunofluorescent visualization of arrays of transverse cortical actin microfilaments in wheat root-tip cells. Protoplasma 147, 204–206.

McMichael CM, Bednarek SY (2013). Cytoskeletal and membrane dynamics during higher plant cytokinesis. New Phytol 197, 1039–1057.

Mineyuki Y (1999). The preprophase band of microtubules: its function as a cytokinetic apparatus in higher plants. Inter Rev Cytol 187, 1–49.

Mineyuki Y, Marc J, Palevitz BA (1989). Development of the preprophase band from random cytoplasmic microtubules in guard mother cells of *Allium cepa* L. Planta 178, 291–296.

Mineyuki Y, Palevitz BA (1990). Relationship between preprophase band organization, F-actin and the division site in *Allium*. J Cell Sci 97, 283–295.

Mineyuki Y, Wick SM, Gunning BES (1988). Preprophase bands of microtubules and the cell-cycle: kinetics and experimental uncoupling of their formation from the nuclear-cycle in onion root-tip cells. Planta 174, 518–526.

Mineyuki Y, Yamashita M, Nagahama Y (1991). $p34^{cdc2}$ kinase homologue in the preprophase band. Protoplasma 162, 182–186.

Murata T, Karahara I, Kozuka T, Thomas HG Jr, Staehelin LA, Mineyuki Y (2002). Improved method for visualizing coated pits, microfilaments, and microtubules in cryofixed and freeze-substituted plant cells. J Electron Microsc (Tokyo) 51, 133–136.

Palevitz BA (1987). Actin in the preprophase band. J Cell Biol 104, 1515–1519.

Palevitz BA (1988). Cytochalasin-induced reorganization of actin in *Allium* root cells. Cell Motil Cytoskeleton 9, 283–298.

Panteris E, Apostolakos P, Galatis B (1992). The organization of F-actin in root tip cells of *Adiantum capillus-veneris* throughout the cell cycle. A double label fluorescencemicroscopy study. Protoplasma 170, 128–137.

Panteris E, Galatis B, Quader H, Apostolakos P (2007). Cortical actin filament organization in developing and functioning stomatal complexes of *Zea mays* and *Triticum turgidum*. Cell Motil Cytoskeleton 64, 531–548.

Petrasek J, Schwarzerova K (2009). Actin and microtubule cytoskeleton interactions. Curr Opin Plant Biol 12, 728–734.

Pickett-Heaps JD, Northcote DH (1966a). Cell division in the formation of the stomatal complex of the young leaves of wheat. J Cell Sci 1, 121–128.

Pickett-Heaps JD, Northcote DH (1966b). Organization of microtubules and endoplasmic reticulum during mitosis and cytokinesis in wheat meristems. J Cell Sci 1, 109–120.

Preuss ML, Kovar DR, Lee YR, Staiger CJ, Delmer DP, Liu B (2004). A plant-specific kinesin binds to actin microfilaments and interacts with cortical microtubules in cotton fibers. Plant Physiol 136, 3945–3955.

Rodriguez OC, Schaefer AW, Mandato CA, Forscher P, Bement WM, Waterman-Storer CM (2003). Conserved microtubule-actin interactions in cell movement and morphogenesis. Nat Cell Biol 5, 599–609.

Sampathkumar A, Lindeboom JJ, Debolt S, Gutierrez R, Ehrhardt DW, Ketelaar T, Persson S (2011). Live cell imaging reveals structural associations between the actin and microtubule cytoskeleton in arabidopsis. Plant Cell 23, 2302–2313.

Sano T, Higaki T, Oda Y, Hayashi T, Hasezawa S (2005). Appearance of actin microfilament "twin peaks" in mitosis and their function in cell plate formation, as visualized in tobacco BY-2 cells expressing GFP-fimbrin. Plant J 44, 595–605.

Schneider R, Persson S (2015). Connecting two arrays: the emerging role of actin-microtubule cross-linking motor proteins. Front Plant Sci 6, 415.

Seagull RW, Heath IB (1979). The effects of tannic acid on the in vivo preservation of microfilaments. Eur J Cell Biol 20, 184–188.

Sinnott EW (1960). Plant Morphogenesis, New York: McGraw-Hill.

Staiger CJ, Cande WZ (1991). Microfilament distribution in maize meiotic mutants correlates with microtubule organization. Plant Cell 3, 637–644.

Staiger CJ, Poulter NS, Henty JL, Franklin-Tong VE, Blanchoin L (2010). Regulation of actin dynamics by actin-binding proteins in pollen. J Exp Bot 61, 1969–1986.

Takeuchi M, Mineyuki Y (2014). Actin-microtubule interaction during preprophase band formation in onion root tips visualized by immunofluorescence microscopy. In: Atlas of Plant Cell Structure, ed. T Noguchi, S Kawano, H Tsukaya, S Matsunaga, A Sakai, I Karahara, and Y Hayashi, Tokyo: Springer-Verlag, 132, Plate 6.13.

Tiwari SC, Polito VS (1988). Organization of the cytoskeleton in pollen tubes of *Pyrus communis*: a study employing conventional and freeze-substitution electron microscopy, immunofluorescence, and rhodamin-phalloidin. Protoplasma 147, 100–112.

Tiwari SC, Wick SM, Williamson RE, Gunning BES (1984). Cytoskeleton and integration of cellular function in cells of higher-plants. J Cell Biol 99, S63–S69.

Traas JA, Doonan JH, Rawlins DJ, Shaw PJ, Watts J, Lloyd CW (1987). An actin network is present in the cytoplasm throughout the cell cycle of carrot cells and associates with the dividing nucleus. J Cell Biol 105, 387–395.

Wick SM, Duniec J (1983). Immunofluorescence microscopy of tubulin and microtubule arrays in plant-cells. 1. Preprophase band development and concomitant appearance of nuclear envelope-associated tubulin. J Cell Biol 97, 235–243.

Wick SM, Duniec J (1984). Immunofluorescence microscopy of tubulin and microtubule arrays in plant-cells. 2. Transition between the pre-prophase band and the mitotic spindle. Protoplasma 122, 45–55.

Xu T, Qu Z, Yang X, Qin X, Xiong J, Wang Y, Ren D, Liu G (2009). A cotton kinesin GhKCH2 interacts with both microtubules and microfilaments. Biochem J 421, 171–180.

Zachariadis M, Quader H, Galatis B, Apostolakos P (2001). Endoplasmic reticulum preprophase band in dividing root-tip cells of *Pinus brutia*. Planta 213, 824–827.